



Small-angle scattering of polychromatic X-rays: effects of bandwidth, spectral shape and high harmonics

Sen Chen^a and Sheng-Nian Luo^{a,b*}

Received 7 August 2017

Accepted 22 December 2017

Edited by A. F. Craievich, University of São Paulo, Brazil

Keywords: SAXS; polychromatic; size distribution; undulator light source.

^aThe Peac Institute of Multiscale Sciences, Chengdu, Sichuan 610031, People's Republic of China, and ^bKey Laboratory of Advanced Technologies of Materials, Ministry of Education, Southwest Jiaotong University, Chengdu, Sichuan 610031, People's Republic of China. *Correspondence e-mail: sluo@pims.ac.cn

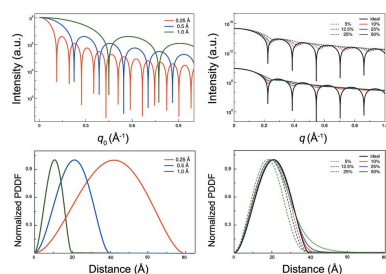
Polychromatic X-ray sources can be useful for photon-starved small-angle X-ray scattering given their high spectral fluxes. Their bandwidths, however, are 10–100 times larger than those using monochromators. To explore the feasibility, ideal scattering curves of homogeneous spherical particles for polychromatic X-rays are calculated and analyzed using the Guinier approach, maximum entropy and regularization methods. Monodisperse and polydisperse systems are explored. The influence of bandwidth and asymmetric spectra shape are explored *via* Gaussian and half-Gaussian spectra. Synchrotron undulator spectra represented by two undulator sources of the Advanced Photon Source are examined as an example, as regards the influence of asymmetric harmonic shape, fundamental harmonic bandwidth and high harmonics. The effects of bandwidth, spectral shape and high harmonics on particle size determination are evaluated quantitatively.

1. Introduction

As a non-destructive method, small-angle X-ray scattering (SAXS) is useful for determining evolution dynamics of particle-scale characteristics such as particle size and shape, and folding status during irreversible transient processes at submicrometer scales (Aleksenskii *et al.*, 1999; Titov *et al.*, 2007; Ten *et al.*, 2012), including nucleation and growth of nanoparticles in phase transitions, detonation and catalytic reactions, and nanovoids in cavitation and spallation. Third-generation synchrotron X-ray sources and X-ray free-electron lasers offer promise for *in situ* single-pulse or short-exposure-time SAXS measurements (Gustavsen *et al.*, 2017; Bagge-Hansen *et al.*, 2015; Willey *et al.*, 2017; Wang *et al.*, 2015a; Bediako *et al.*, 2017; Takahashi *et al.*, 2017; Chen *et al.*, 2017).

In conventional SAXS measurements, monochromatic X-ray beams with a bandwidth of $\Delta E/E \simeq 10^{-4}$ are usually used. Here, E denotes photon energy. For synchrotron light sources, such a monochromaticity is usually achieved with single-crystal monochromators such as Si(111) double crystals, at the expense of effective spectral flux. Consequently, a long exposure time is required to ensure sufficiently high signal-to-noise ratios, but is undesirable for photon-starved measurements. A hard X-ray free-electron laser, with higher flux and fully transverse coherence (Lehmkuhler *et al.*, 2015), can achieve simultaneously higher monochromaticity (10^{-2} – 10^{-3}) and high temporal resolution (10–100 fs), but its general user time is extremely limited.

Despite its high spectral flux, the bandwidth of an undulator source without a monochromator is usually 10–100 times



larger than that in conventional SAXS (Wang *et al.*, 2015*b*). Such a limited polychromaticity may still render severe smearing in the scattering curves, and introduce additional uncertainties in determining particle size distributions. The influence of polychromaticity on structure determination in SAXS was explored, but only symmetric Gaussian spectra and monodisperse systems were considered (Wang *et al.*, 2015*b*). Analytical resolution functions considering various instrumentation smearing effects have been derived (Ramakrishnan, 1985; Moore, 1980), but symmetric Gaussian spectra are the most studied (Pedersen *et al.*, 1990; Pedersen & Riekel, 1991). Such symmetric spectra with a wavelength spread up to 10–20% are common in neutron scattering measurements since mechanical velocity selectors are used. However, for synchrotron undulator sources used for dynamic measurements (Ihee, 2008; Luo *et al.*, 2012), asymmetric harmonic shape may lead to a more smeared scattering pattern. In some measurements with full spectra, high harmonics may also affect the scattering curves. The effects of spectral shape and high harmonics have not been evaluated with resolution function yet. Desmearing such scattering curves is highly desirable, and various strategies have been proposed to introduce corrections into data reduction, including stabilized Mellin transforms (Svergun & Semeniuk, 1985, 1986), iteration (Lake, 1967) and indirect Fourier transform (Glatter, 1974; Moore, 1980).

Recently, there has been an increased interest in conducting such ‘pink beam’ SAXS measurements at a synchrotron facility, such as the beamline 32-ID of Advanced Photon Source (APS; Argonne, IL, USA), which is dedicated to dynamic X-ray diffraction/scattering and imaging experiments. An open question is how reliable particle size (for monodisperse systems) or size distribution (for polydisperse systems) can be resolved in the presence of smearing solely due to polychromaticity. In this work, we investigate the influence of polychromatic X-rays on SAXS measurements. For completeness, both shape and high harmonics effects are examined for monodisperse and polydisperse nanoparticle systems. We demonstrate certain feasibility of SAXS measurements with synchrotron light sources such as the APS undulator sources without a monochromator and additional desmearing.

2. Methodology

We consider dilute isotropic systems consisting of randomly distributed spherical particles with a particle size distribution function $W_R(R)$, and a ‘pink beam’ light source with a spectral function $W_\lambda(\lambda)$. The corresponding scattering intensity, $I(q)$, can be written as (Feigin & Svergun, 1987; Dreiss *et al.*, 2006)

$$I(q) = \int_0^\infty \int_0^\infty W_R(R) T(\lambda) W_\lambda(\lambda) \Delta\rho^2 V^2(R) \times F^2(q\lambda_0/\lambda, R) d\lambda dR, \quad (1)$$

where R , V , λ and λ_0 are the particle radius, particle volume, wavelength of the incident beam and reference wavelength, respectively. T denotes transmission, and $\Delta\rho$ is the scattering length density and is related to the real part of the atomic scattering factor. The amplitude of the scattering vector is $q = 4\pi \sin \theta/\lambda_0$. $F(q, R)$, the form factor amplitude of a homogeneous sphere with radius R , is

$$F(q, R) = 3 \frac{\sin qR - qR \cos qR}{(qR)^3}. \quad (2)$$

Energy dependence of the atomic scattering factor for X-rays (Fox *et al.*, 1989) is not considered in equation (1) and the discussion below, since it varies little at small angles.

The wavelength-dependent transmission for X-rays, $T(\lambda)$, can be readily considered by introducing $W'_\lambda(\lambda) = T(\lambda) W_\lambda(\lambda)$, where $W'_\lambda(\lambda)$ is the transmission modulated spectral function. In this work, we focus on the simplest case with $T(\lambda) = 1$. Detector efficiency can be treated similarly (Dreiss *et al.*, 2006), but it is beyond the scope of this work.

Monochromatic light sources with different wavelengths, Gaussian and half-Gaussian spectral functions with different bandwidths, and spectra of two undulator light sources of the APS with periods of 33 mm (U33) and 18 mm (U18) are considered. Monochromatic sources illustrate how SAXS profiles and corresponding results are influenced by spectral components with longer or shorter wavelength λ than the reference wavelength λ_0 . A Gaussian spectral function (Fig. 1*a*) is used to reveal the influence of the bandwidth, and a half-Gaussian function (Fig. 1*b*) is used to investigate the effect of asymmetric harmonic shape which is common in undulator light sources. Spectra of U18 and U33 (Fig. 2) are simulated with *XOP* and APS undulator parameters (Sanchez del Rio & Dejus, 2004; Ilinski *et al.*, 1996; Luo *et al.*, 2012).

Energy spectra of U33 and U18 with different undulator gaps (Fig. 2) both consist of fundamental and high harmonics,

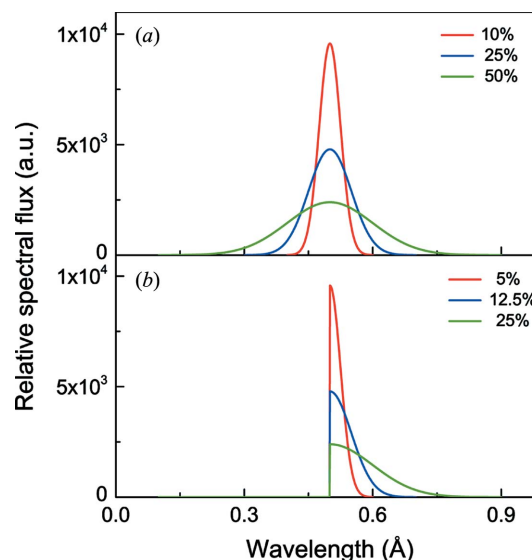


Figure 1 Gaussian and half-Gaussian X-ray spectra with different bandwidths as noted. The reference wavelength is 0.5 Å.

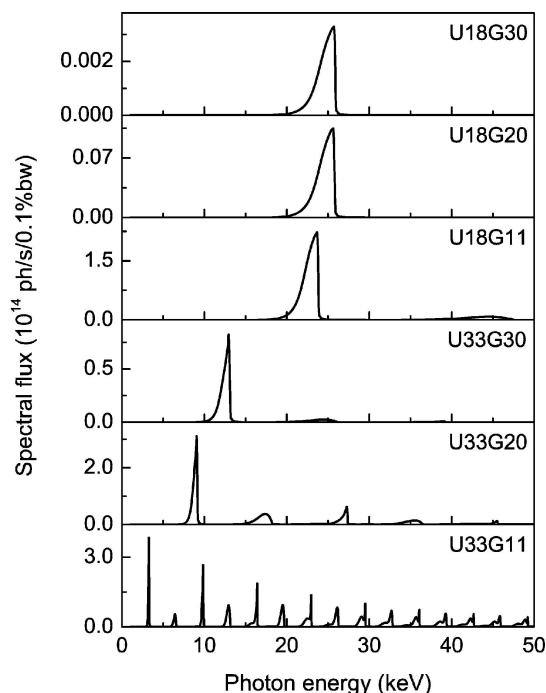


Figure 2
Simulated spectral photon flux through a 1 mm × 1 mm area located at 35 m away from the source, for APS undulators U33 and U18 with different gaps (11 mm, 20 mm, 30 mm). The electron energy is 7 GeV and the current is 100 mA.

and all harmonics are asymmetric. For U18, high harmonics are considerably weaker than the fundamental. With increasing undulator gap, spectral fluxes decrease rapidly and the bandwidth of each harmonic widens. For photon-starved SAXS measurements, we need as many photons and smaller bandwidth as possible, so smaller gaps are preferred. However, as undulator gap decreases, higher harmonics become stronger (Fig. 2), which may lead to marked smearing of scattering curves.

Monodisperse and polydisperse systems are explored. For the monodisperse system, the particle radius is set to be 20 Å. Particle sizes of the polydisperse system follow a Gaussian distribution function centered at $R = 20$ Å with a standard deviation of 4 Å. Preset particle size distribution and related particle volume distribution function (PVDF) are shown in Fig. 3, and PVDF centers at about 22 Å.

For monodisperse systems, the radius of gyration, R_g , of primary particles is obtained under the Guinier approximation as

$$I(q) = I(0) \exp(-R_g^2 q^2 / 3) \quad (3)$$

for $qR_g \leq 1.3$. Particle radius R follows as $R = \sqrt{5/3}R_g$ for homogeneous spherical particles.

The pair distance distribution function (PDDF), $p(r)$, can be calculated using

$$p(r) = \frac{1}{2\pi^2} \int_0^\infty I(q) q r \sin(qr) dq. \quad (4)$$

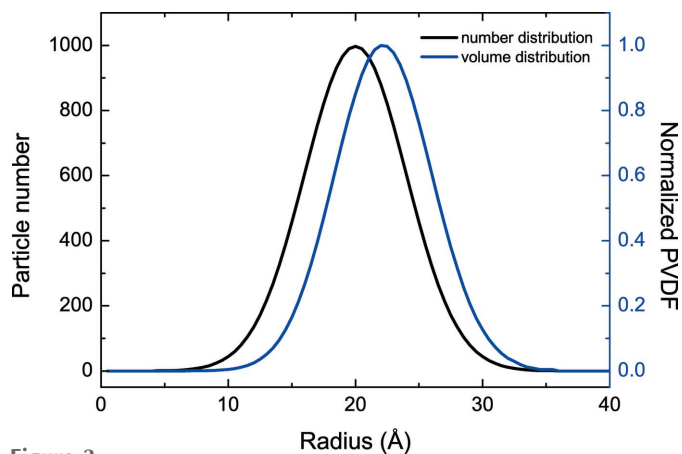


Figure 3
Preset distribution functions of a size-polydisperse system, in terms of particle size distribution (black curve) and normalized PVDF (blue curve).

In this work, the regularization method as implemented in the SAXS package *Irena* (Ilavsky & Jemian, 2009) is used to retrieve the corresponding PDDFs.

Retrieving particle size distributions from SAXS profiles is a typical linear inverse problem. Given measured quantities d_i ($i = 1, 2, \dots, M$), one searches for a set of numbers x_j ($j = 1, \dots, N$), which is linearly related to d_i . The maximum entropy (MaxEnt) (Jemian *et al.*, 1991; Potton *et al.*, 1988) and regularization are two methods implemented in the SAXS analysis package *Irena* (Ilavsky & Jemian, 2009) for obtaining size distributions of a polydisperse system. In fact, both MaxEnt and regularization methods perform optimization of parameters with the constraint $\chi^2 = M$. Here, χ^2 describes the goodness of fit,

$$\chi^2 = \sum_{i=1}^M (d_i - y_i)^2 / \sigma_i, \quad (5)$$

where σ_i and y_i are the standard deviation of the measurement d_i and the predicted intensity, respectively.

For the MaxEnt method, a solution to this inverse problem is obtained *via* maximizing the configurational entropy,

$$S = - \sum_{j=1}^N x_j \log(x_j / b_j). \quad (6)$$

Here b_j is a prescribed scaling value for x_j , and x_j is the fraction of particles of size j described by a particle size histogram. In the regularization method, the smoothness of a calculated size distribution is maximized *via* minimizing the sum of squared curvature deviations (Ilavsky & Jemian, 2009).

3. Results and discussion

Monodisperse and polydisperse systems consisting of randomly distributed spherical particles are explored. Monochromatic light with different wavelengths of 0.25 Å, 0.5 Å and 1.0 Å, Gaussian spectral functions with bandwidths of 10%, 25% and 50%, half-Gaussian spectral functions with bandwidths of 5%, 12.5% and 25%, and APS undulator light

sources with periods of 33 mm and 18 mm are examined. The reference wavelength λ_0 is 0.5 Å for monochromatic, Gaussian and half-Gaussian source spectra. For undulator sources, different magnet gaps are considered, and the reference wavelength is where the intensity of a fundamental peaks. For instance, a gap of 11 mm is denoted as G11. R_g of primary particles in a monodisperse system is obtained with the Guinier approximation, and PDDFs are derived with the regularization method. PVDFs of size polydisperse systems are derived with the MaxEnt and regularization methods. The resultant maximum and full width at half-maximum (FWHM) of a PVDF are obtained and compared for different source spectra.

3.1. Monodisperse system

A monodisperse system with a particle radius of 20 Å (corresponding to $R_g = 15.5$ Å) is explored. Simulated SAXS profiles for different X-ray source spectra are presented in Fig. 4. Source parameters and Guinier analysis results are listed in Table 1.

3.1.1. Monochromatic light. Relative to a reference wavelength, reducing/increasing the wavelength leads to contraction/expansion of the scattering curves (Fig. 4a), and expansion/contraction of the PDDFs (Fig. 4d). For wavelengths shorter than λ_0 , the left-shift of minima due to reduced wavelength would be attributed to larger particle size if we assume the same wavelength (λ_0) for polychromatic X-rays, leading to an overestimate of R_g . It is the opposite for longer wavelengths. Indeed, Table 1 shows that the particle size is

Table 1

Source parameters and particle radius (R) obtained from the Guinier analysis for a monodisperse system (preset particle radius $R_0 = 20$ Å). Asterisks (*) indicate that only the fundamentals are considered.

Spectrum	λ_0 (Å)	Bandwidth (%)	R (Å)	$(R - R_0)/R_0$ (%)
0.25 Å	0.5	0	40.4	100.2
0.5 Å	0.5	0	20.3	1.5
1.0 Å	0.5	0	10.0	-50.0
Gaussian	0.5	10	20.4	2.0
Gaussian	0.5	25	20.6	3.0
Gaussian	0.5	50	21.2	6.0
Half-Gaussian	0.5	5	19.6	-2.0
Half-Gaussian	0.5	12.5	18.9	-5.5
Half-Gaussian	0.5	25	17.7	-11.5
U18G11	0.53	-	21.1	5.0
U33G11	3.80	-	>100.0	>400.0
U33G20	1.37	-	32.6	63.0
U33G30	0.96	-	21.5	7.5
U18G11*	0.53	7.7	19.4	-3.0
U18G20*	0.48	7.8	19.4	-3.0
U18G30*	0.48	8.5	19.3	-3.5
U33G11*	3.80	2.3	20.1	0.5
U33G20*	1.37	5.2	19.7	-1.5
U33G30*	3.80	6.3	19.6	-2.0

overestimated or underestimated by a factor of 2 when λ is reduced by half or doubled. Since the total scattering for polychromatic spectra is the linear combination of scattering for different wavelengths [equation (1)], this analysis with monochromatic light demonstrates how scattering curves are affected by different spectral components.

3.1.2. Symmetric spectra. A symmetric spectrum contains competing components contributing to an over- or under-

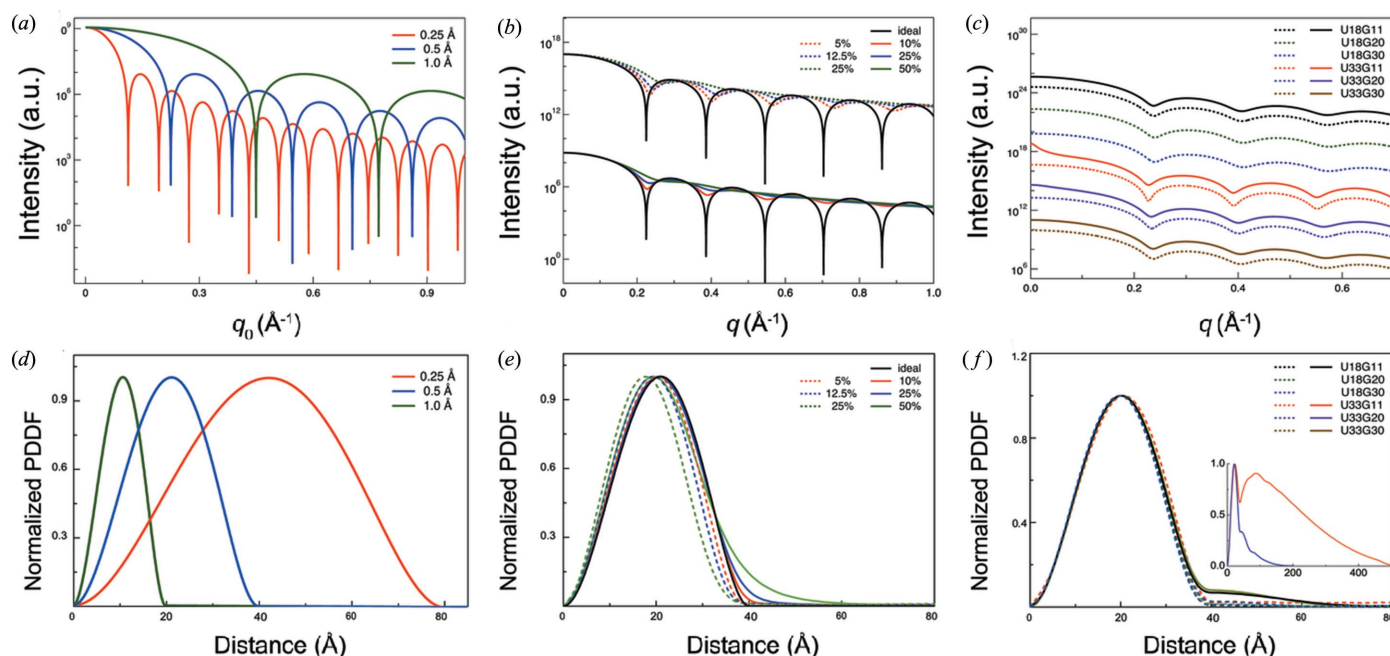


Figure 4 Simulated small-angle scattering curves (upper row) and corresponding PDDFs (bottom row) of a monodisperse system with a particle radius of 20 Å for different X-ray sources. (a), (d) Monochromatic light with different wavelengths (0.25 Å, 0.5 Å and 1.0 Å). Curves are plotted as a function of q_0 , i.e. the q -values expected for the reference wavelength. (b), (e) Gaussian spectra (solid lines) with bandwidths of 10%, 25% and 50%, half-Gaussian spectra (dotted lines) with bandwidths of 5%, 12.5% and 25%, and an ideal monochromatic light source (black line). The reference wavelengths are all 0.5 Å. (c), (f) Undulator light sources, APS U33 and U18, at different undulator gaps. Calculations use a full spectrum (solid line) and the first harmonic (dashed line) for each case except U18G20 and U18G30. Inset in (f): PDDFs calculated with the full spectra of U33G11 and U33G20.

estimate in particle size, and, overall, leads to an overestimate, since the contribution of shorter wavelengths outruns that of longer wavelengths. The results for Gaussian functions (Fig. 1*a*) with different bandwidths are listed in Table 1, and show overall an overestimated R_g , consistent with a previous study (Wang *et al.*, 2015*b*). The overestimate increases with increasing bandwidth, being 2%, 3% and 6% for bandwidths of 10%, 25% and 50%, respectively. Although the Guinier approach yields larger R_g , the minima in Fig. 4(*b*) shift to higher q , corresponding to smaller particles. At low q values, the contribution of longer wavelengths varies little while that of shorter wavelengths decreases rapidly, so the total scattering intensity decreases more quickly than the ideal one, leading to larger R_g when the Guinier approach is used. At high q , the contribution of shorter wavelengths decreases much more quickly than that for longer wavelengths, and longer-wavelength components play a more important role, so the minima shift to higher q . Symmetric spectra lead to an increase of maximum dimension, and the maximum of PDDF shifts to a shorter distance (Fig. 4*e*).

3.1.3. Asymmetric spectra. Asymmetric half-Gaussian spectra (Fig. 1*b*) with a spectral shape similar to that of the harmonics of undulator light sources (Fig. 2) at beamline 32-ID-B of APS are examined. As described above, lower-energy (longer-wavelength) components gives rise to an underestimated R_g and thus R (Table 1). As the bandwidth increases from 5% to 25%, the underestimate in R_g increases from 2.0% to 11.5%. Again, longer-wavelength components in the spectra lead to a shift of PDDF maxima to shorter distances, as observed in Fig. 4(*e*).

3.1.4. Undulator light sources of the APS. For U18 and U33 with different undulator gaps, we calculate SAXS profiles with fundamentals only and with full spectra. For U18 operated at gaps of 20 mm and 30 mm, only the fundamental is considered since higher harmonics are considerably weaker. In the case of strong absorption, $T(\lambda)$ changes the relative contributions of different harmonics. The contributions from higher harmonics become relatively larger due to their higher transmission, leading to a more distorted scattering curve and greater overestimation of particle size while using the Guinier approach.

For full spectra, the scattering curves are smeared (Fig. 4*c*) as a result of the presence of higher harmonics and finite bandwidths of all harmonics. For U33, a high harmonic with stronger intensity leads to more distortion in the low- q segment of a scattering curve, which in turn gives rise to a steeper slope and thus larger R_g from the Guinier analysis. When only the fundamentals are considered, the spectral shape plays a vital role and leads to an underestimate of particle size as discussed for the asymmetric spectra. The last six cases in Table 1 indicate that the underestimation in R_g increases with

increasing bandwidth. It should be stressed that, for monodisperse systems, even a weak second harmonic might impact the resultant R_g considerably when the Guinier approach is used. Therefore, for such SAXS measurements, rejecting high harmonics cleanly is necessary.

3.2. Polydisperse system

A size polydisperse system with a Gaussian size distribution (Fig. 3) is explored. Such high polydispersity can be found in dynamic processes like catalytic combustion (Wang *et al.*, 2015*a*) and high explosives detonation (Kuznetsov *et al.*, 1994). Low-dispersity systems show similar results, and therefore are not presented here. Monochromatic beams, Gaussian and half-Gaussian spectra with different bandwidths, and undulator sources of U33 and U18 are used as well. Size distribution functions are analyzed *via* the MaxEnt and regularization methods implemented in the package *Irena*, and presented as PVDFs.

3.2.1. Monochromatic light. Three wavelengths, 0.25 Å, 0.5 Å and 1.0 Å, are explored and the results are presented in Fig. 5. The reference wavelength is $\lambda_0 = 0.5$ Å.

As shown above for monochromatic X-rays in §3.1 for monodisperse systems, shorter- or longer-wavelength components lead to squeezed ($\lambda < \lambda_0$) or stretched ($\lambda > \lambda_0$) profiles, and, correspondingly, R_g is overestimated or underestimated. This effect is also observed for a polydisperse system: the profiles are squeezed/stretched (Fig. 5*a*), and related PVDFs are stretched/squeezed as a result (Fig. 5*b*). With such stretching or squeezing of PVDFs, FWHMs of resolved PVDFs become greater/smaller than the preset value, and the value of R corresponding to the maximum PVDF is overestimated/underestimated (Table 2).

For systems with a Gaussian size distribution, and monochromatic X-rays with wavelength λ and reference wavelength λ_0 , FWHM and R can be estimated by

$$\text{FWHM} = \text{FWHM}_0(\lambda_0/\lambda) \tag{7}$$

and

$$R = R_0(\lambda_0/\lambda), \tag{8}$$

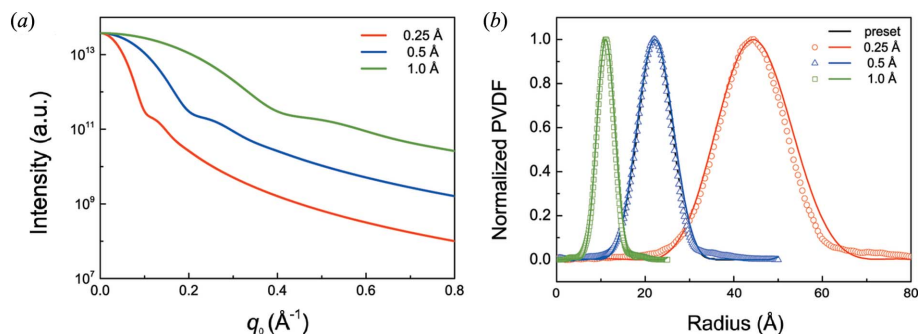


Figure 5 Scattering curves and PVDFs for a polydisperse system with the Gaussian size distribution shown in Fig. 3, for monochromatic X-rays. (*a*) Simulated SAXS profiles for different wavelengths of 0.25 Å, 0.5 Å and 1.0 Å. (*b*) Corresponding PVDFs obtained with the MaxEnt (symbols) and regularization (solid lines) methods.

Table 2

Source parameters and particle radius (R) obtained with the MaxEnt and regularization methods for the polydisperse system.

R and FWHM refer to the maximum and the FWHM of PVDFs, respectively. Asterisks (*) indicate that only the fundamentals are considered.

Spectrum	Bandwidth (%)	MaxEnt				Regularization			
		R (Å)	ΔR (%)	FWHM (Å)	$\Delta FWHM$ (%)	R (Å)	ΔR (%)	FWHM (Å)	$\Delta FWHM$ (%)
Preset	–	22.0	–	9.0	–	22.0	–	9.0	–
0.25 Å	0.0	44.5	102.3	17.5	94.4	44.5	102.3	19.8	120.0
0.5 Å	0.0	22.0	0.0	8.9	–1.1	22.1	0.5	9.6	6.7
1.0 Å	0.0	11.1	–49.5	4.3	–52.2	11.1	–49.5	4.8	–46.7
Gaussian	10.0	22.0	0.0	9.0	0.0	22.1	0.5	11.2	24.4
Gaussian	25.0	20.9	–5.0	9.5	5.6	21.6	–1.8	12.0	33.3
Gaussian	50.0	18.7	–15.0	10.6	17.8	19.7	–10.5	13.6	51.1
Half-Gaussian	5.0	21.1	–4.1	8.5	–5.6	21.4	–2.7	10.5	16.7
Half-Gaussian	12.5	20.2	–8.2	8.5	–5.6	20.4	–7.3	10.6	17.8
Half-Gaussian	25.0	17.9	–18.6	8.9	–1.1	18.7	–15.0	11.1	23.3
U18G11	–	20.9	–5.0	8.7	–3.3	21.2	–3.6	10.5	16.7
U33G11	–	22.0	0.0	8.9	–1.1	22.0	0.0	10.8	20.0
U33G20	–	21.0	–4.5	8.6	–4.4	22.0	0.0	13.4	48.9
U33G30	–	20.5	–6.8	8.6	–4.4	21.5	–2.3	12.0	33.3
U18G11*	7.7	20.9	–5.0	8.7	–3.3	21.2	–3.6	10.5	16.7
U18G20*	7.8	20.6	–6.4	8.7	–3.3	20.9	–5.0	10.6	17.8
U18G30*	8.5	20.6	–6.4	8.7	–3.3	20.9	–5.0	10.4	15.6
U33G11*	2.3	21.7	–1.4	8.8	–2.2	22.0	0.0	9.9	10.0
U33G20*	5.2	21.2	–3.6	8.8	–2.2	21.4	–2.7	10.3	14.4
U33G30*	6.3	20.9	–5.0	8.8	–2.2	21.2	–3.6	10.7	18.9

where $FWHM_0$ and R_0 are the FWHM and central value of the preset PVDF, respectively.

In addition, different analysis methods for size distribution also yield different PVDFs. For instance, FWHM obtained from the MaxEnt method appears to be smaller than that from the regularization method.

3.2.2. Gaussian and half-Gaussian spectra. A broader bandwidth leads to more smearing in scattering curves (Fig. 6a). Symmetric spectra result in an overestimation of particle size obtained with the Guinier approach, in contrast to the Gaussian and half-Gaussian cases for monodisperse systems. All resultant PVDFs of polydisperse systems are left-shifted, indicating an underestimation of particle sizes obtained with the MaxEnt and regularization methods; and such an underestimation increases with increasing bandwidth.

For polydisperse systems, symmetric spectra result in an underestimation of particle size with the profile fitting

methods, in contrast to the Gaussian cases for monodisperse systems analyzed with the Guinier approach.

For asymmetric spectra such as the half-Gaussian spectra examined here, the asymmetry results in a much more severe underestimation of particle sizes obtained with profile fitting, consistent with the results in §3.2.1. With increasing bandwidth, the underestimation increases as well (Table 2).

3.2.3. Source U18 of APS. The bandwidth of a U18 source, as well as the energy of the fundamental, varies slightly as the undulator gap increases (Fig. 2 and Table 2). For gaps of 20 mm and 30 mm, only the fundamentals are considered since they dominate high harmonics in spectral flux. As a result, the scattering profiles for different undulator gaps are similar (Fig. 7a).

PVDFs are extracted using the MaxEnt (Fig. 7b) and regularization (Fig. 7c) methods. Both methods overestimate the FWHMs of PVDFs for a Gaussian size distribution, and

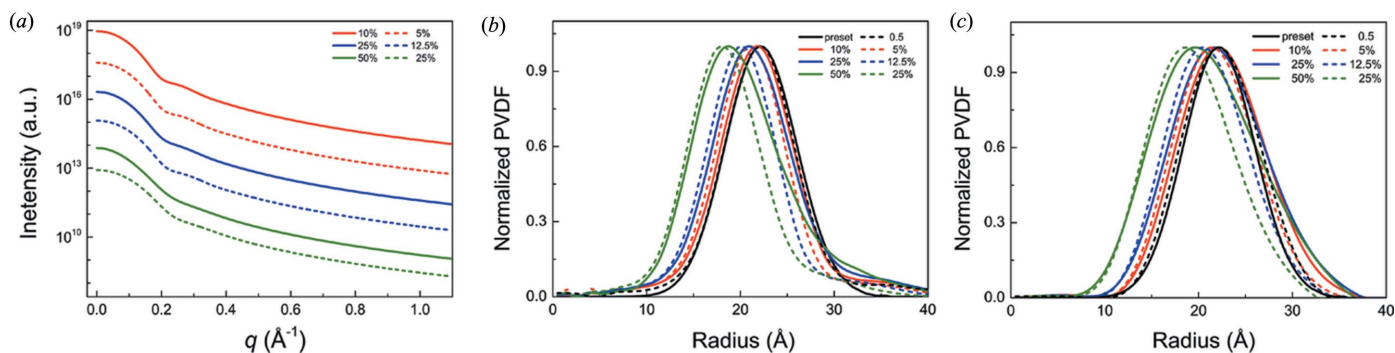


Figure 6 Scattering curves and PVDFs for a polydisperse system with the Gaussian size distribution as shown in Fig. 3, for Gaussian (solid lines) and half-Gaussian (dashed lines) spectra. (a) Simulated SAXS profiles for different bandwidths, and corresponding PVDFs obtained with (b) the MaxEnt and (c) regularization methods.

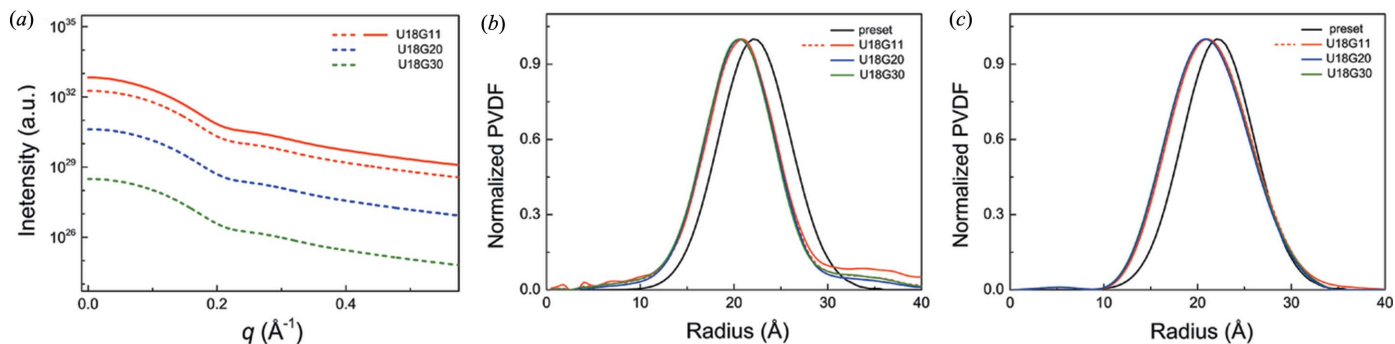


Figure 7 Scattering curves and PVDFs for a polydisperse system with the Gaussian size distribution as shown in Fig. 3, for undulator sources of U18 at different gaps (11 mm, 20 mm, 30 mm). Full spectra (solid lines) and fundamentals (dashed line) are considered separately. (a) Simulated SAXS profiles, and corresponding PVDFs obtained with (b) the MaxEnt and (c) regularization methods.

FWHMs obtained from the MaxEnt method are smaller than those from the regularization method. The bandwidth and the asymmetric shape of a fundamental give rise to underestimated particle sizes as described in §3.2.2. Differences in PVDFs due to different gaps are negligible.

Even at the smallest undulator gap (11 mm) where high harmonics cannot be neglected, the results are still acceptable (Table 2). In fact, errors are less than -5.0% in R for both MaxEnt and regularization methods, and those in FWHMs are less than 10% and 20% for the MaxEnt and regularization methods, respectively. Such accuracy is reasonable for many photon-starved SAXS measurements. It is also encouraging that all these results are based on full spectrum calculation. Thus, no additional monochromators or filters, or desmearing procedures, are needed. SAXS measurements for dynamic experiments or even single-shot experiments appear to be feasible with U18 sources at different gaps (as low as 11 mm).

3.2.4. Source U33 of APS. To some extent, U33 is better in monochromaticity, since its fundamentals have narrower bandwidths than U18 (Table 2). However, its high harmonics are much stronger than those of U18, and impact SAXS severely as discussed in §3.1. As expected, the initial part of the scattering curves in Fig. 8(a) are distorted considerably due to the existence of higher harmonics. Such a distortion results in an overestimation of particle sizes obtained with the Guinier approach. However, for the profile fitting methods

such as MaxEnt and regularization, high harmonics present themselves in a different way.

For a spectrum consisting of strong high harmonics (harmonic number $j \geq 2$), a much wider fitting range is needed (Figs. 8b and 8c) for profile fitting. Otherwise the deviation between a fitted profile and the fitting would be unacceptable. Given the existence of higher harmonics, profile fitting yields nonexistent larger particles, while the Guinier analysis simply overestimates particle size. The results listed in Table 2 for U33 spectra are calculated for the first peak of PVDFs. Suppose that components of an undulator spectrum are discrete, and the wavelength at the maximum spectral flux is set as the reference wavelength λ_0 . Then, the wavelength for the j th harmonic can be approximated as

$$\lambda_j = \lambda_0 / j. \quad (9)$$

At a given scattering angle θ , the scattering intensity contributed by the j th harmonic, I_j , is expressed in terms of the scattering vector $q = 4\pi \sin \theta / \lambda_0$ as

$$I_j(q, R) = W_R(R) T(\lambda_j) W_\lambda(\lambda_j) \times \left[3\Delta\rho V \frac{\sin(qR\lambda_0/\lambda_j) - qR\lambda_0/\lambda_j \cos(qR\lambda_0/\lambda_j)}{(qR\lambda_0/\lambda_j)^3} \right]^2. \quad (10)$$

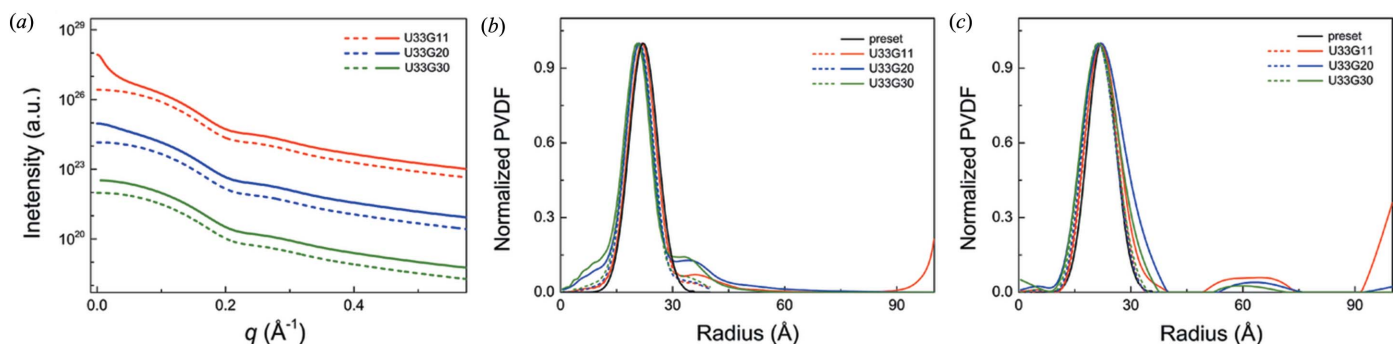


Figure 8 Scattering curves and PVDFs for a polydisperse system with the Gaussian size distribution as shown in Fig. 3, for undulator sources of U33 at different gaps (11 mm, 20 mm, 30 mm). Full spectra (solid lines) and fundamentals (dashed line) are considered separately. (a) Simulated SAXS profiles, and corresponding PVDFs obtained with (b) the MaxEnt and (c) regularization methods.

Substitute λ_j [equation (9)] and $V = (4/3)\pi R^3$ into equation (10), and let $jR = R_j$. Then equation (10) becomes

$$I_j(q, R) = W_R(R) T(\lambda_j) W_\lambda(\lambda_j) j^{-6} \times \left(4\pi \Delta\rho \frac{\sin qR_j - qR_j \cos qR_j}{q^3} \right)^2 = j^{-6} I_j(q, R_j). \quad (11)$$

Equation (11) indicates that the contribution of the j th harmonic to the total scattering curve is exactly the same as that of particles with particle radius jR . The corresponding total particle number or effective spectral flux for such nonexistent particles is reduced by a factor of j^{-6} . As an example, for $j = 3$, the effective spectral flux is reduced to below 0.2% of the incident spectra. In other words, the contribution of a high harmonic decreases rapidly as j increases, so we only need to take the first one or two harmonics into account even when a full undulator bandwidth is used. Consistently, the PVDFs in Figs. 8(b) and 8(c) demonstrate that the volume fractions of those nonexistent particles with larger radii are quite small, compared with the PVDF peak which is due to the fundamental or first harmonic. When mirrors or refractive lenses are used, higher harmonics are significantly rejected (Polikarpov *et al.*, 2014; Timmann *et al.*, 2009), so one need consider only the first harmonic. On the other hand, when transmission is considered, $T(\lambda)$ increases as λ decreases, and j^{-6} becomes $j^{-6}T(\lambda)$. Contributions from higher harmonics become stronger when $T(\lambda)$ is considered.

Although both the MaxEnt and regularization methods yield nonexistent particles of bigger sizes, their PVDFs are quite different in the large- R regime. As presented in Figs. 8(b) and 8(c), the MaxEnt method gives rise to a more continuous PVDF distribution in this regime. However, the regularization method, similar to equation (10), produces nonexistent particles with radius jR .

Higher harmonics do not cause a considerable overestimation of R obtained with the profile fitting methods. This can be verified by comparing the results of full spectra and fundamentals for U33 (Table 2). Similar to the U18 case, the asymmetric shape and bandwidth of harmonics give rise to underestimation of R . Different from U18, the bandwidth of a U33 fundamental is much smaller and, unsurprisingly, the related errors in R and FWHM are also smaller.

The regularization and MaxEnt methods overestimate and underestimate FWHMs of the resultant PVDFs for U18 and U33, regardless of whether a full spectrum or only the first harmonic is used.

4. Summary

We have investigated systematically the influence of polychromatic X-rays on SAXS measurements and their interpretation. Typical characteristics of synchrotron undulator spectra such as bandwidth, asymmetric harmonic shape and high harmonics are considered. Data reduction methods such as the Guinier approach for monodisperse systems, and the

MaxEnt and regularization methods for polydisperse systems, are explored for SAXS interpretation. The effects of bandwidth, symmetric/asymmetric spectral shape and high harmonics on particle size determination are investigated quantitatively with realistic undulator sources.

Acknowledgements

We benefited from valuable discussions with Drs K. Fezzaa and T. Sun at the Advanced Photon Source.

Funding information

Funding for this research was provided by: National Key R&D Program of China (grant No. SQ2017YFGX090020-02); National Natural Science Foundation of China (grant No. 11627901).

References

- Aleksenskii, A. E., Baidakova, M. V., Vul', A. Y. & Siklitskii, V. (1999). *Phys. Solid State*, **41**, 668–671.
- Bagge-Hansen, M., Lauderbach, L., Hodgkin, R., Bastea, S., Fried, L., Jones, A., van Buuren, T., Hansen, D., Benterou, J., May, C., Graber, T., Jensen, B. J., Ilavsky, J. & Willey, T. M. (2015). *J. Appl. Phys.* **117**, 245902.
- Bediako, H., Smith, A. D., Ukogu, O., Dasgupta, M., White, E. & Carter, A. R. (2017). *Biophys. J.* **112**, 371a.
- Chen, Y., Tokuda, J. M., Topping, T., Meisburger, S. P., Pabit, S. A., Gloss, L. M. & Pollack, L. (2017). *Proc. Natl Acad. Sci.* **114**, 334–339.
- Dreiss, C. A., Jack, K. S. & Parker, A. P. (2006). *J. Appl. Cryst.* **39**, 32–38.
- Feigin, L. & Svergun, D. (1987). *Structure Analysis by Small-Angle X-ray and Neutron Scattering*. New York: Plenum Press.
- Fox, A. G., O'Keefe, M. A. & Tabbernor, M. A. (1989). *Acta Cryst.* **A45**, 786–793.
- Glatter, O. (1974). *J. Appl. Cryst.* **7**, 147–153.
- Gustavsen, R., Dattelbaum, D., Watkins, E., Firestone, M., Podlesak, D., Jensen, B., Ringstrand, B., Huber, R., Mang, J., Johnson, C., Velizhanin, K. A., Willey, T. M., Hansen, D. W., May, C. M., Hodgkin, R. L., Bagge-Hansen, M., van Buuren, A. W., Lauderbach, L. M., Jones, A. C., Graber, T. J., Sinclair, N., Seifert, S. & Gog, T. (2017). *J. Appl. Phys.* **121**, 105902.
- Ihee, H. (2009). *Acc. Chem. Res.* **42**, 356–366.
- Ilavsky, J. & Jemian, P. R. (2009). *J. Appl. Cryst.* **42**, 347–353.
- Ilinski, P., Dejus, R. J., Gluskin, E. & Morrison, T. I. (1996). *Proc. SPIE*, **2856**, 16–25.
- Jemian, P., Weertman, J., Long, G. & Spal, R. (1991). *Acta Metall. Mater.* **39**, 2477–2487.
- Kuznetsov, V., Chuvilin, A., Moroz, E., Kolomiichuk, V., Shaikhutdinov, S. K., Butenko, Y. V. & Mal'kov, I. Y. (1994). *Carbon*, **32**, 873–882.
- Lake, J. A. (1967). *Acta Cryst.* **23**, 191–194.
- Lehmkuhler, F., Kwaśniewski, P., Roseker, W., Fischer, B., Schroer, M. A., Tono, K., Katayama, T., Sprung, M., Sikorski, M., Song, S., Glowina, J., Chollet, M., Nelson, S., Robert, A., Gutt, C., Yabashi, M., Ishikawa, T. & Grübel, G. (2015). *Sci. Rep.* **5**, 17193.
- Luo, S. N., Jensen, B. J., Hooks, D. E., Fezzaa, K., Ramos, K. J., Yeager, J. D., Kwiatkowski, K. & Shimada, T. (2012). *Rev. Sci. Instrum.* **83**, 073903.
- Moore, P. B. (1980). *J. Appl. Cryst.* **13**, 168–175.
- Pedersen, J. S., Posselt, D. & Mortensen, K. (1990). *J. Appl. Cryst.* **23**, 321–333.
- Pedersen, J. S. & Riekel, C. (1991). *J. Appl. Cryst.* **24**, 893–909.

- Polikarpov, M., Snigireva, I. & Snigirev, A. (2014). *J. Synchrotron Rad.* **21**, 484–487.
- Potton, J. A., Daniell, G. J. & Rainford, B. D. (1988). *J. Appl. Cryst.* **21**, 663–668.
- Ramakrishnan, V. (1985). *J. Appl. Cryst.* **18**, 42–46.
- Sanchez del Rio, M. & Dejus, R. J. (2004). *Proc. SPIE*, **5536**, 171–174.
- Svergun, D. & Semeniuk, A. (1985). *Dokl. Akad. Nauk SSSR*, **284**, 621–626.
- Svergun, D. & Semenyuk, A. (1986). *Stud. Biophys.* **112**, 255–262.
- Takahashi, R., Narayanan, T. & Sato, T. (2017). *J. Phys. Chem. Lett.* **8**, 737–741.
- Ten, K., Prueel, E. & Titov, V. (2012). *Fullerenes, Nanotubes Carbon Nanostructures*, **20**, 587–593.
- Timmann, A., Döhrmann, R., Schubert, T., Schulte-Schrepping, H., Hahn, U., Kuhlmann, M., Gehrke, R., Roth, S. V., Schropp, A., Schroer, C. & Lengeler, B. (2009). *Rev. Sci. Instrum.* **80**, 046103.
- Titov, V., Tolochko, B., Ten, K., Lukyanchikov, L. & Prueel, E. (2007). *Diamond Relat. Mater.* **16**, 2009–2013.
- Wang, J., Seifert, S., Winans, R. E., Tolmachoff, E., Xin, Y., Chen, D., Wang, H. & Anderson, S. L. (2015a). *J. Phys. Chem. C*, **119**, 19073–19082.
- Wang, W., Shtykova, E. V., Volkov, V. V., Chang, G., Zhang, L., Dong, Y. & Liu, P. (2015b). *J. Appl. Cryst.* **48**, 1935–1942.
- Willey, T., Bagge-Hansen, M., Lauderbach, L., Hodgkin, R., Hansen, D., May, C., van Buuren, T., Dattelbaum, D., Gustavsen, R., Watkins, E., Firestone, M. A., Jensen, B. J., Graber, T., Bastea, S. & Fried, L. (2017). *AIP Conf. Proc.* **1793**, 030012.